https://doi.org/10.5194/egusphere-2024-1109
Preprint. Discussion started: 17 April 2024
© Author(s) 2024. CC BY 4.0 License.

The effect of stiffness contrasts at faults on stress orientation

Moritz O. Ziegler[1,2], Robin Seithel[3], Thomas Niederhuber[4], Oliver Heidbach[2,5], Thomas Kohl[4], Birgit Mueller[4], Mojtaba Rajabi[6], Karsten Reiter[7], and Luisa Roeckel[4]

[1]Technical University Munich, Arcisstraße 21, 80333 Munich, Germany
[2]Helmholtz Centre Potsdam GFZ German Research Centre for Geosciences, Telegrafenberg, 14473 Potsdam, Germany
[3]GHJ - Ingenieurgesellschaft für Geo- und Umwelttechnik mbH & Co. KG, Am Hubengut 4, 76149 Karlsruhe, Germany
[4]Institute of Applied Geosciences, KIT, 76131 Karlsruhe, Germany
[5]Institute for Applied Geosciences, TU Berlin, 10587 Berlin, Germany
[6]School of the Environment, University of Queensland, 4072 Saint Lucia, Queensland, Australia
[7]Institute of Applied Geosciences, TU Darmstadt, 64287 Darmstadt, Germany

Correspondence: Moritz O. Ziegler (moritz.ziegler@tum.de)

Abstract. Even though the crustal stress state is primarily driven by gravitational volume forces and plate tectonics, interpretations of borehole breakout observations show occasionally abrupt rotations of horizontal stress orientation of up to 90° when faults are crossed. This indicates the influence of faults on the local stress state, which parameter control the degree of rotation. Herein, we investigate the phenomenon of principal stress rotation at a fault by means of a 2D generic numerical model. We parametrised the fault as a rock stiffness contrast and investigate systematically the full model parameter space in terms of the ratio of the applied principal stresses, the rock stiffness contrast, as well as the angle between fault strike and orientation of the principal stress axis. General findings are that the stress rotation is negatively correlated with the ratio of principal stresses. A small angle between the far field stress orientation and the fault facilitates stress rotation. A high contrast in rock stiffness further increases the stress rotation angle. Faults striking perpendicular to the maximum principal stress orientation experience no rotation at all. However, faults oriented parallel to the maximum principal stress orientation experience either no rotation or a 90° rotation, dependent on the ratio of principal stresses and the rock stiffness contrast. A comparison with observations from various boreholes worldwide shows that in general, the findings are well in agreement, even though the dip angle proves to have an influence on the stress rotation, in particular for shallow dipping faults.

1 Introduction

The contemporary crustal stress state is a key parameter for the stability assessment of subsurface operations, such as the extraction of raw materials, storage of waste and usage of geothermal energy (Catalli et al., 2013; Müller et al., 2018; van Wees et al., 2018). Most frequently available stress information is the orientation of the maximum horizontal stress component S_{Hmax} which is compiled in the World Stress Map (Heidbach et al., 2018). Often, the S_{Hmax} orientation is observed to be consistent over large areas and volumes following the general patterns imposed by plate tectonics (Han et al., 2019; Heidbach et al., 2018; Rajabi et al., 2017a; Reiter et al., 2014), but regionally variable patterns are also observed (Konstantinou et al., 2017; Niederhuber et al., 2023; Ziegler et al., 2016c). In addition, the S_{Hmax} orientation pattern is influenced by topography of large

https://doi.org/10.5194/egusphere-2024-1109
Preprint. Discussion started: 17 April 2024
© Author(s) 2024. CC BY 4.0 License.

mountain ranges (Levi et al., 2019; Reinecker et al., 2010; Zoback, 1992) or sedimentary basin geology (Rajabi et al., 2016a, b; Snee and Zoback, 2018). Furthermore, it has also been hypothesized that the S_{Hmax} orientation is diverted by faults (Dart and Swolfs, 1992; Faulkner et al., 2006; Konstantinovskaya et al., 2012; Li et al., 2023; Schoenball et al., 2018; Yale, 2003). However, Reiter et al. (2024) showed with a comprehensive study using a generic geomechancial model that fault induced stress changes beyond a distance of a few hundred meters from the fault core are too small to be resolved by stress data.

Nevertheless, on a meter scale in boreholes abrupt or gradual rotations of the S_{Hmax} orientation have been observed (Barton and Zoback, 1994; Brudy et al., 1997; Massiot et al., 2019; Sahara et al., 2014; Shamir and Zoback, 1992; Wang et al., 2023). Over the last decade, a great increase in high-resolution image logs in various basins across the world, provides the opportunity for detailed observation of such small-scale stress rotations in the vicinity of faults at borehole scales (Lin et al., 2010; Rajabi et al., 2022, 2024; Sahara et al., 2014; Talukdar et al., 2022; Zhang et al., 2023). Figure 1a shows an example of stress re-orientation of approximately 90° indicated by borehole breakouts (Bell and Gough, 1979; Heidbach et al., 2018) in the vicinity of and attributed to a fault, which has been interpreted in an electrical image log in the Surat Basin of Queensland, Australia (Rajabi et al., 2017a).

The observed change in breakout orientation is the manifestation of a change in the orientation of the maximum circumferential stress at the borehole wall (Figure 1b) which is a function of the position at the borehole wall with respect to the orientation of the principal stresses components S_1, S_2, and S_3 (Kirsch, 1898). The principal stress components result from the transformation of the 2nd order symmetric stress tensor

$$\sigma_{ij} = \begin{pmatrix} \sigma_{xx} & \sigma_{yx} & \sigma_{zx} \\ \sigma_{xy} & \sigma_{yy} & \sigma_{zy} \\ \sigma_{xz} & \sigma_{yz} & \sigma_{zz} \end{pmatrix} \tag{1}$$

into the main axis system (2), where the three remaining components are the three principal stresses that are perpendicular to each other, and it is defined that $S_1 > S_2 > S_3$.

$$\sigma = \begin{pmatrix} S_1 & 0 & 0 \\ 0 & S_2 & 0 \\ 0 & 0 & S_3 \end{pmatrix} \tag{2}$$

Any changes in the magnitudes of the individual components of the stress tensor σ_{ij} are transmitted by the main axis transformation to the three principal stress components. However, only changes in the deviatoric stress tensor (Engelder, 1994) components can potentially change the principal stress axes orientation (Figure 1b). This is commonly referred to as stress rotation. It can be observed e.g., as a change in the orientation of borehole breakouts (Figure 1a).

Even though stress rotations can be observed in boreholes under some circumstances, knowledge of where to expect stress rotations is important for subsurface operations that specifically target faults for their permeable properties (Freymark et al., 2019; Konrad et al., 2021) or may avoid them for the same reasons but still will encounter them (Gilmore et al., 2022; Long and Ewing, 2004). This raises the questions which parameters are decisive for a stress rotation and how sensitive they are.

https://doi.org/10.5194/egusphere-2024-1109
Preprint. Discussion started: 17 April 2024
© Author(s) 2024. CC BY 4.0 License.

The possibility and angle of a stress rotation is commonly assumed to be mainly dependent on the smallest and largest principal stress components S_1 and S_3, usually considered in terms of the differential stress S_1-S_3 (Reiter, 2021; Sonder, 1990; Ziegler et al., 2017). Furthermore, the angle of the fault strike represented by a rock stiffness contrast with respect to the orientation of S_{Hmax} is expected to influence the stress rotation (Reiter, 2021; Siler, 2023). Several additional parameters such as rock fabric and geological structures (i.e., faults and fractures) have been suggested as the possible causes of these stress re-orientations at small scales (Faulkner et al., 2006; Hung et al., 2007; Siler, 2023; Yale, 2003). This is observed at various locations worldwide where boreholes have been drilled through faults while observations of the stress state were possible (e.g., Brudy et al., 1997; Cui et al., 2014; Hickman and Zoback, 2004; Lin et al., 2007). While some faults exhibit a rotation of up to 90° (Lin et al., 2007), others show significantly less (Cui et al., 2014; Hickman and Zoback, 2004) or considering the uncertainties almost no rotation at all (Yamada and Shibanuma, 2015).

We investigate the reason for this diverse behaviour from a geomechanical perspective and investigate the influence of various parameters on the angle of stress rotation. We focus on the near field of the fault and the damage zone, i.e., the volume around the fault where the rock is significantly fractured and affected in its integrity. We expect a substantial influence of the far field stress field in terms of the differential stress as shown in previous studies (Reiter, 2021; Sonder, 1990; Ziegler et al., 2017) but also in terms of the stress ratio $R_S=S_1/S_3$. Furthermore, the contrast in material properties is the basis for any stress rotation and in particular the stiffness (Young's modulus) is demonstrated to have a significant influence (Hergert et al., 2015; Reiter, 2021; Ziegler, 2022). Eventually, the angle between the fault strike and the orientation of S_{Hmax} is investigated as an influential parameter (Reiter et al., 2024; Siler, 2023).

We use a generic geomechanical-numerical model that allows a systematic and comprehensive investigation of the model parameter space in terms of stiffness contrast, stress ratio, and angle of the fault with respect to the far field stress state. We focus on the near field of the fault at scales of 10s of meters and limit the investigation to the linear elastic response of the stress state to rock stiffness contrasts which has not been investigated in previous studies that focused on processes (Ziegler et al., 2017), did not investigate the full range of parameters (Reiter, 2021) and methods of fault representation due to a different objective (Reiter et al., 2024). Herein, we conduct an exhaustive study and investigate the entire parameter space.

2 Model setup

In order to investigate the stress rotation at a fault we set up a 2D plane strain model of a fault in a strike slip stress regime, i.e., $S_1=S_{Hmax}$ and $S_2=S_{hmin}$. The dimension of the numerical model is 10 x 10 km^2 with a central 5 m wide fault that dissects the entire model (Figure 2a). We use the finite element method to solve the problem numerically and the model is discretized in a way that boundary effects and numerical artefacts are reduced (Homberg et al., 1997; Spann et al., 1994).

Within the fault, plane strain quad-elements form a finite element mesh with a resolution of 5 m along strike and 0.25 m normal to the fault strike. These elements represent the fault by a rock stiffness that is different to that of the host rock. The 200 m at each side of the fault are also discretized by quad-elements (Figure 2c). The element size normal to the fault strike increases with distance from the fault. Outside the immediate vicinity of the fault, plane strain tria-elements with a mesh

https://doi.org/10.5194/egusphere-2024-1109
Preprint. Discussion started: 17 April 2024
© Author(s) 2024. CC BY 4.0 License.

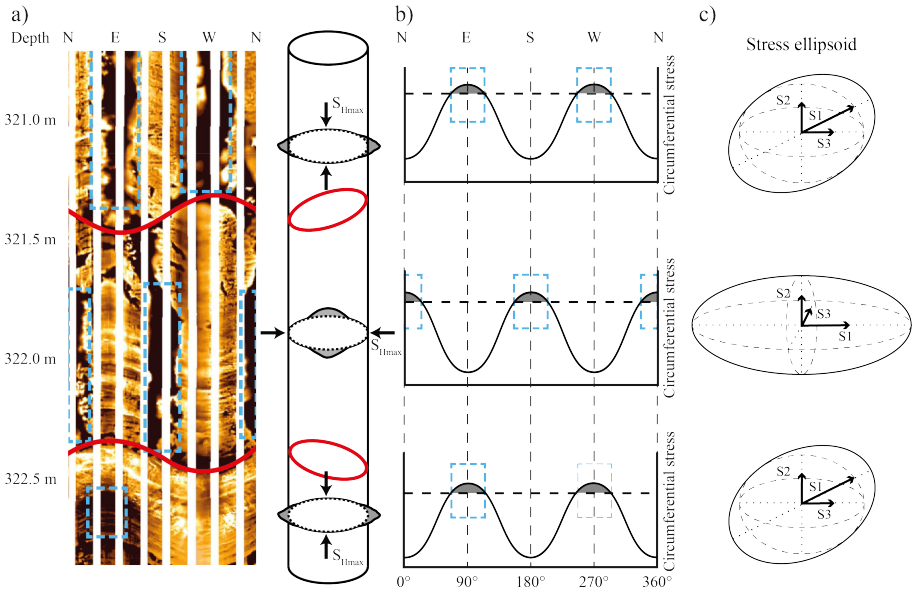

Figure 1. An example of stress rotation due to the presence of a small-scale fault in a borehole. The regional S_{Hmax} orientation in the vicinity of this well of approx. 0° (Mukherjee et al., 2020; Rajabi et al., 2017a) is indicated by borehole breakouts (black areas in image log) oriented East-West above and below the fault zone delineated by the two sinusoidal red lines. The part in between shows the section that is affected by the fault and thus shows a rotated stress state. a) Borehole breakouts (blue dashed lines) interpreted in a resistivity image log in the Kenya East Well in the Surat Basin, Eastern Australia and the borehole diameter represented in 3D. Dark areas represent conductive zones where the borehole is elongated and light areas zones of high resistivity. b) Variations of the circumferential stress at the borehole wall (bold sinusoidal line) with the orientations where the compressive strength (dashed horizontal line) is exceeded (grey areas) and breakouts occur (dashed blue lines). c) Representation of the stress tensor above and below the fault with the stress ellipsoid visualizing orientations and magnitudes of the three principal stresses S_1, S_2, and S_3.

coarsening to 100 m at the boundary are used (Figure 2b). The total number of elements of the model is variable depending on the model set up, but it is always in the order of about 75,000 elements. The stress state of the model is controlled with displacement boundary that are chosen in such a way that they result in the desired horizontal stress magnitudes (Figure. 2a)(Ziegler et al., 2023).

To evaluate which parameter controls the amount of stress rotation, we systematically vary the stiffness contrast between the fault and the host rock, the ratio of principal stresses $R_S=S_1/S_2$, and the angle γ between the faults strike and the far-field S_1 orientation (Table 1). For the host rock we choose a Young's modulus Ehost=40 GPa and a Poisson's ratio of 0.25 and for the fault, the stiffness is systematically varied between Efault=0.4 GPa and Efault=40 GPa, resulting in 13 scenarios with a rock stiffness contrast R_E=Efault/Ehost between 0.01 and 1. This corresponds to a range of a very soft fault up to the non-existence of a fault. The Poisson's ratio was kept constant at 0.25 as the influence of the stiffness is considered as the most important parameter, as shown by previous studies (Reiter, 2021; Ziegler, 2022). We test the influence of the material contrast in eleven

https://doi.org/10.5194/egusphere-2024-1109
Preprint. Discussion started: 17 April 2024
© Author(s) 2024. CC BY 4.0 License.

Table 1. Range of parameters investigated in this study. Note that the rock stiffness contrast R_E has a step width of 0.1 (4 GPa) between a R_E=1 and R_E=0.1. Larger contrasts are realised to be 0.07, 0.04, and 0.01. The host rock always has a Young's modulus of Ehost=40 GPa. The stress ratio Rs, the differential stress S_1-S_2, and the absolute stress magnitudes are indicated. γ is the angle between fault strike and S_1 orientation that varies between 0° (parallel) and 90° (perpendicular). The results of all computations are provided in the supplementary material.

Parameter	Values													Num. scen.
R_E	1	0.9	0.8	0.7	0.6	0.5	0.4	0.3	0.2	0.1	0.07	0.04	0.01	13
E_{fault} [GPa]	40	36	32	28	24	20	16	12	8	4	2.8	1.6	0.4	
$R_S=S_1/S_2$	1.0	1.1	1.2	1.3	1.4	1.5	1.6	1.7	1.8	1.9	2.0			11
S_1-S_2 [MPa]	0.00	2.25	5.00	8.25	12.00	16.25	21.00	26.25	32.00	38.25	45.00			
S_1 [MPa]	20.00	24.75	30.00	35.75	42.00	48.75	56.00	63.75	72.00	80.75	90.00			
S_2 [MPa]	20.0	22.5	25.0	27.5	30.0	32.5	35.0	37.5	40.0	42.5	45.0			
γ [°]	0	5	10	15	20	25	30	35	40	45	50	55	60	65	70	75	80	85	90	19

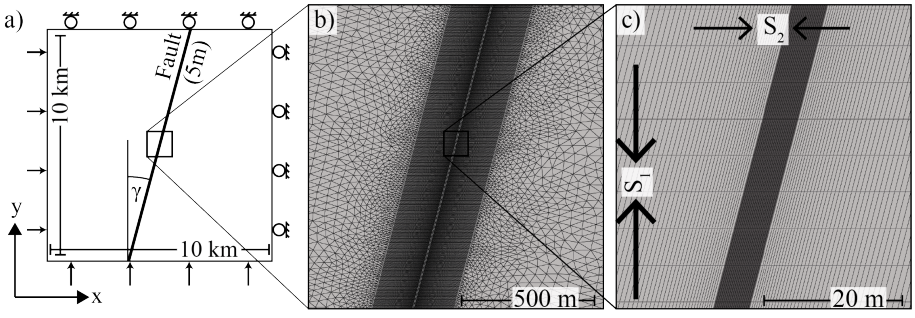

Figure 2. Sketch of the model setup. a) Conceptual setup of the generic 2D model with the applied boundary conditions and the location of the fault in the centre of the model. Please note that the fault can be rotated in 5° steps. b) Detailed excerpt that shows the refined mesh geometry in the fault core and close to the fault. An area of 200 m on either side of the fault is discretised with quadrilateral elements for a better resolution. c) Closeup of the fault (dark area) and its immediate vicinity (light area) that shows the high resolution of 25 cm normal to the fault strike and 5 m in fault strike direction. Please not that S_1=S_{Hmax} and S_2=S_{hmin}.

95 far field principal stress ratios. We iterate the angle γ from 0° to 90° in 5°-steps. For the full parameter space this results in total in 2717 model scenarios that are solved and then analysed.

https://doi.org/10.5194/egusphere-2024-1109
Preprint. Discussion started: 17 April 2024
© Author(s) 2024. CC BY 4.0 License.

3 Results

The model results provide at the nodes of the finite elements the normal stress components σxx and σyy in orientation of the x- and y-axes, respectively, and the shear stress component σxy. The orientation of S_1 in the far-field from the fault is parallel to the y-axis. In order to obtain the angle of stress rotation we determine the change of the S_1 and S_2 orientation in the centre of the fault.

The stress rotation for a fault with an angle γ = 15°, a moderate R_E=0.4 (16 GPa fault, 40 GPa host rock), and a principal stress ratio R_S=1.4 (S_1 = 35 MPa, S_2 = 25 MPa, S_1-S_2 = 10 MPa) is displayed in Figure 3a. There, a clockwise rotation of the principal stress axes by 59° can be observed in the fault centre. Outside this zone, the principal stress orientations adhere to the far field stress state as no visual rotation can be observed (Figure 3a).

In order to test the hypothesis that the three parameters, the angle γ, the rock stiffness contrast R_E, and the relative stress magnitudes of S_1 and S_2 influence the stress rotation angle, each of them is changed and the results are observed in comparison to Figure 3a. A decrease of the stress ratio to R_S=1.2 while S_1-S_2 remains leads to an increased stress rotation (Figure 3b). An increase in S_1-S_2 from 10 MPa to 30 MPa (S_1 = 105 MPa, S_2 = 75 MPa) while R_S remains the same results in the same rotation angle of 59° (Figure 3c). In contrast, an increase in S_1-S_2 to 30 MPa with a change in R_S=1.75 results in a decrease of stress rotation to 45° (Figure 3d). This indicates that it is rather the stress ratio R_S that controls the stress rotation than the differential stress. A more comprehensive comparison is shown in Table 2.

A reduction of R_E=0.4 to R_E=0.7 means that the fault is stiffer and thus closer to the host rocks stiffness. This results in an even larger reduction of the stress rotation by 31° to 28° (Figure 3e). This positive correlation of rock stiffness contrast R_E to potential stress rotation angle has been observed previously (Reiter, 2021). It is intuitive in that with the herein made assumptions the same stiffness in fault and host rock (R_E=1) cannot lead to any rotation at all. Thus, the larger R_E is, the smaller is the expected stress rotation.

An increase in the angle γ between the fault strike and the far-field S_1 orientation from initially 15° to now 45° results in a smaller rotation angle of 19° (Figure 3f). The angle γ is thus negatively correlated with the rotation angle. No rotation is expected for faults that strike perpendicular to the S_{Hmax} orientation (γ=90°).

As already indicated in Figure 3, stress rotation is observed only directly in the fault zone where a rock stiffness contrast R_E exists. In order to systematically investigate its influence we investigate the stress rotation as a function of distance normal to the fault. No significant changes in the orientation of S_1 can be observed outside the fault (Figure 4). However, significantly different stress rotation angles are observed within the fault dependent on the R_E value following the observations made in Figure 3b and e.

Furthermore, within the contrasting rock volumes there is no gradual difference observed between the borders and the centre (Figure 4). Only at the border between fault and host rock, an intermediate stress rotation angle can be observed. This apparent stress rotation should not be interpreted as it is a result of the interpolation from the integration points within the elements to the nodes. At material contrasts it is thus a mixture of stress states from the two bounding lithologies and its extent depends on

https://doi.org/10.5194/egusphere-2024-1109
Preprint. Discussion started: 17 April 2024
© Author(s) 2024. CC BY 4.0 License.

the discretization. It can be disregarded in the following analysis. Thus, in the following we refer to the stress rotation in the centre of the model and the fault only. This allows to display the results in a more comprehensive way (Figure 5).

Four different stress ratios R_S are compared in Figure 5 which highlights the importance of the angle γ. Structures with a significant contrast in rock stiffness that are perpendicular to the far field orientation of S_1 (γ=90°) do not exhibit any rotation of the principal stress axes at all. In turn, structures parallel to the S_1 orientation (γ=0°) may exhibit the maximally possible stress rotation of 90° which signifies a mutual replacement of S_1 and S_2 orientation, respectively.

Whether the maximum possible stress rotation of 90° is reached is tied to the ratios R_E and R_S. For large contrasts (i.e. small R_E) and small R_S values, the maximum stress rotation angle is reached in several scenarios. At the same time, high R_E values limit the maximally achieved stress rotation angle. The maximum angle for any given R_E value is then up to 90° and controlled by the stress ratio R_S (Figure 5). However, in these cases the maximum angle is not observed for γ=0° but for angles $0° < \gamma < 45°$. Apparently, for an angle $\gamma = 0°$ either no stress rotation at all or the maximally possible stress rotation of 90° occurs.

The large influence of the R_S value is additionally displayed in a representation of the three model parameters in this study (Figure 6). There, the decisiveness of the R_S value becomes apparent. This is in particular observable for R_E=0.6 at faults that are striking parallel to the S_1 orientation (γ=0°). A low R_S of around 1.1 leads to a stress rotation of 90° (Figure 5a). However, an increase of R_S to ≥ 1.5 (Figure 6) prevents any stress rotation at all.

These results show, that the previously indicated correlations (Figure 3) can be confirmed. This is in particular a negative correlation between R_S and the stress rotation angle, a negative correlation between R_E and the stress rotation angle, and a negative correlation between the angle γ between strike angle vs. far-field S_1 orientation and the stress rotation angle. A general rule that can be observed is that the sum of the angle γ added to the observed stress rotation cannot exceed 90°. Furthermore, no configuration of parameters allows a rotation of 90° if $\gamma > 0°$. Conversely, for $\gamma = 90°$ no investigated configuration allows within the fault core any stress rotation at all.

4 Discussion

The influence of the rock stiffness contrast R_E, the stress ratio R_S, and angle between a fault or in general a geological structure and the far-field S_1 orientation on the rotation of the principal stress axes are derived from a generic study. The results indicate the importance of these factors on the possibility for occurrence and expected angle of stress rotation, which is critical and has numerous implications in energy and resources extraction.

4.1 Application

The occurrence of stress rotation is particularly significant for applications such as geothermal energy, where often faults are specifically targeted for their permeability (Barton et al., 1995; Konrad et al., 2021; Seithel et al., 2015; Siler, 2023). At the same time, these faults potentially host induced seismicity (Gaucher et al., 2015; Schoenball et al., 2014; Seithel et al., 2019). Further geotechnical operations, such as mining and tunnelling, affect the stress state, weaken the rock and lead to stress

https://doi.org/10.5194/egusphere-2024-1109
Preprint. Discussion started: 17 April 2024
© Author(s) 2024. CC BY 4.0 License.

Table 2. Dependence of the stress rotation on the stress ratio R_S. The R_S values are compared with different S_1-S_2 associated with the same angle γ=15° and the same rock stiffness contrast R_E=0.4.

	R_S = 1.2		
S_{1-2} [MPa]	6	10	14
Stress rotation [°]	67.7	67.7	67.7
	R_S = 1.4		
S_{1-2} [MPa]	12	14	18
Stress rotation [°]	59.1	59.1	59.1
	R_S = 1.6		
S_{1-2} [MPa]	18	30	42
Stress rotation [°]	50.5	50.5	50.5
	R_S = 1.8		
S_{1-2} [MPa]	24	40	56
Stress rotation [°]	43.1	43.1	43.1

rotations themselves (Cai et al., 2022; Ptáček et al., 2015; Ziegler et al., 2015) which can lead to rockfall or other damages. Thus, it is of key interest to estimate the potential for these damages such as (induced) seismicity on pre-existing faults.

This requires detailed information on the stress state itself but also the angle of faults with respect to the stress state is crucial (Healy and Hicks, 2022; Morris et al., 1996; Röckel et al., 2022; Worum et al., 2004). Often, a regional stress state obtained from geomechanical models does not include local fault geometries (Ahlers et al., 2022; Clavijo et al., 2024; Gradmann et al., 2024). Then, the modelled stress state is mapped to fault geometries and the according potential for failure is estimated (Röckel et al., 2022; Vadacca et al., 2021; Ziegler et al., 2016a, b). In other instances, faults and their effect on the stress field are included in the model (Hergert et al., 2015; Wees et al., 2003; Xing et al., 2007). However, various different approaches to include faults exist that have different implications for the stress state . (Henk, 2020; Reiter et al., 2024; Treffeisen and Henk, 2020).

This bears the potential that the reactivation potential of a fault is incorrectly estimated if the stress state inside a fault is not or not correctly modelled. This can happen if the far-field stress state is assumed to be the correct stress state inside a fault instead of a rotated far-field stress state. Röckel et al. (2022) potentially indicate this challenge which in some regions could contribute to a mismatch of estimated slip tendency and observed seismicity. Consequently, wrong estimates of the potential for seismicity could be provided by geomechanical models which can lead to severe results. In order to prevent these errors, knowledge of the expected stress rotation as a result of the setting provide a first indication on whether significant rotations of the principal stress axes are expected or not.

https://doi.org/10.5194/egusphere-2024-1109
Preprint. Discussion started: 17 April 2024
© Author(s) 2024. CC BY 4.0 License.

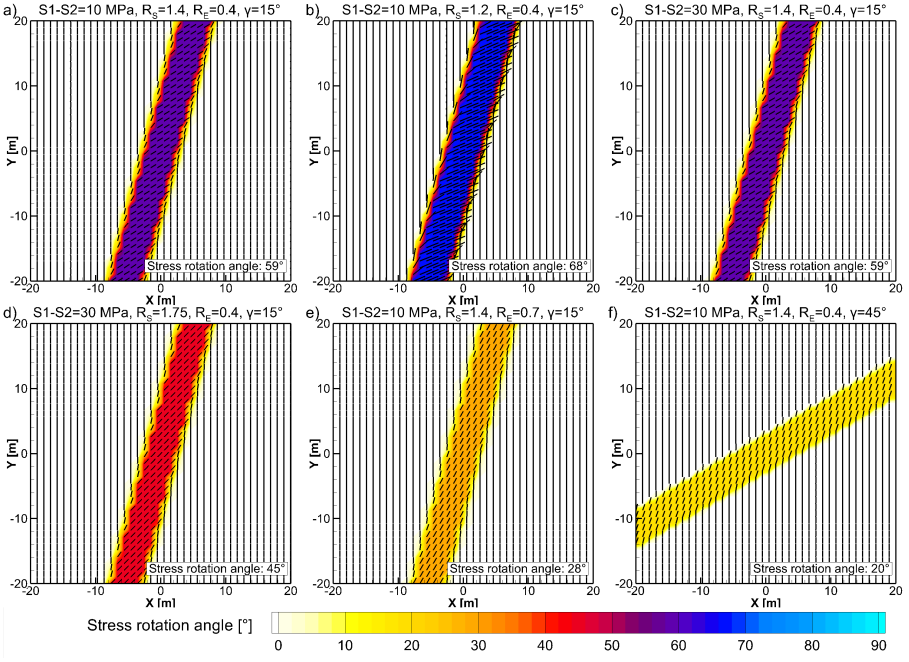

Figure 3. The stress rotation colour-coded and as vectors/lines that indicate the S_1 orientation in the fault core area (Figure 2c) dependent on different settings. a) A basic setting with a fault that is 15° deviated from the orientation of S_1, a differential stress of 10 MPa, a stress ratio of R_S=1.4, and a rock stiffness contrast of R_E=0.4 (E=16 GPa in the fault core and E=40 GPa in the host rock. b) R_S=1.2. c) Differential stress increased to 30 MPa and R_S =1.2. d) Differential stress increased to 30 MPa with the same S_2 magnitude as in a), R_S=1.75. e) R_E=0.7. f) Deviation of 45° between fault strike and the S_1 orientation.

4.2 Implementation

The exact geomechanical behaviour of a fault is difficult to represent in a model since there are various processes involved. The importance and impact of individual processes depends on the purpose of a model. Thus, models tend to implement faults in different ways with a different focus (Henk, 2020; Reiter et al., 2024). Instead of aiming at a realistic representation of a fault, different aspects of a fault properties are commonly investigated individually. This can be the slip behaviour, the plastic deformation, or the alteration of rock properties in the immediate fault core and damage zone (Reiter et al., 2024; Treffeisen and Henk, 2020).

The latter approach is used in this study where the fault is parametrised in terms of a reduction of the stiffness. This follows the assumptions of fault and damage zone that are weakened compared to the host rock (Casey, 1980; Faulkner et al., 2006, 2010; Isaacs et al., 2008) implemented as a reduced Young's modulus. The decision to focus on the rock properties instead of the fault slip was made mainly out of consideration for geotechnical applications that are most likely to target faults that are not expected to slip.

https://doi.org/10.5194/egusphere-2024-1109
Preprint. Discussion started: 17 April 2024
© Author(s) 2024. CC BY 4.0 License.

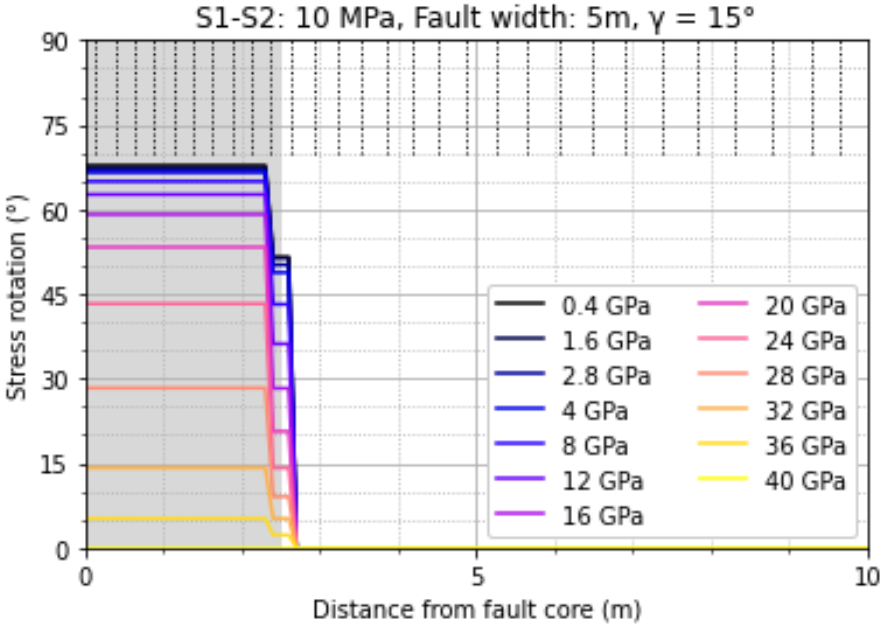

Figure 4. Stress rotation normal to the fault strike dependent on the rock stiffness contrast between the fault's Young's modulus indicated in the legend and a host rock stiffness of Ehost=40 GPa. The distance from the fault core centre (x-axis) in relation to the stress rotation (y-axis). The vertical dotted lines at the top indicate the discretization normal to the fault strike with an element size of 25 cm within the fault and increasing outside the fault. Please note, that the distance is from the fault core centre, thus only half of the fault width is shown here in grey.

4.3 Material gradient

In this study, the fault is realised as a sharp elastic stiffness contrast between the host rock and the fault. When regarding faults, most observations show a gradient between the fault core and the host rock which can be almost a sharp contrast (Barton and Zoback, 1994; Holdsworth et al., 2010) but also consist of several meters of damage zone (Barton and Zoback, 1994; Lockner et al., 2009) or even several tens of meters (Faulkner et al., 2006, 2010; Li et al., 2012; Williams et al., 2016).

In order to investigate the influence of a gradual change in rock properties that mimic the entire fault zone, we implemented in an additional model a linear gradient in rock stiffness perpendicular to the fault strike in the model. The resulting stress rotations outside the fault core agrees with the previous model results and does not show any particular deviations from the previously modelled correlations (Figure 7). It is particularly noteworthy, that the non-linear dependency on the rock stiffness contrast is reflected in the gradual decrease in stress rotation from the fault core towards the host rock.

This shows that the extent of a deviated stress field around a structure with different rock stiffness is dependent on the transition from host rock properties to deviated rock properties. This means that in this simple, generic case the different rock properties in the structure itself are not having any influence on the stress rotation angle beyond its border. However, for a

https://doi.org/10.5194/egusphere-2024-1109
Preprint. Discussion started: 17 April 2024
© Author(s) 2024. CC BY 4.0 License.

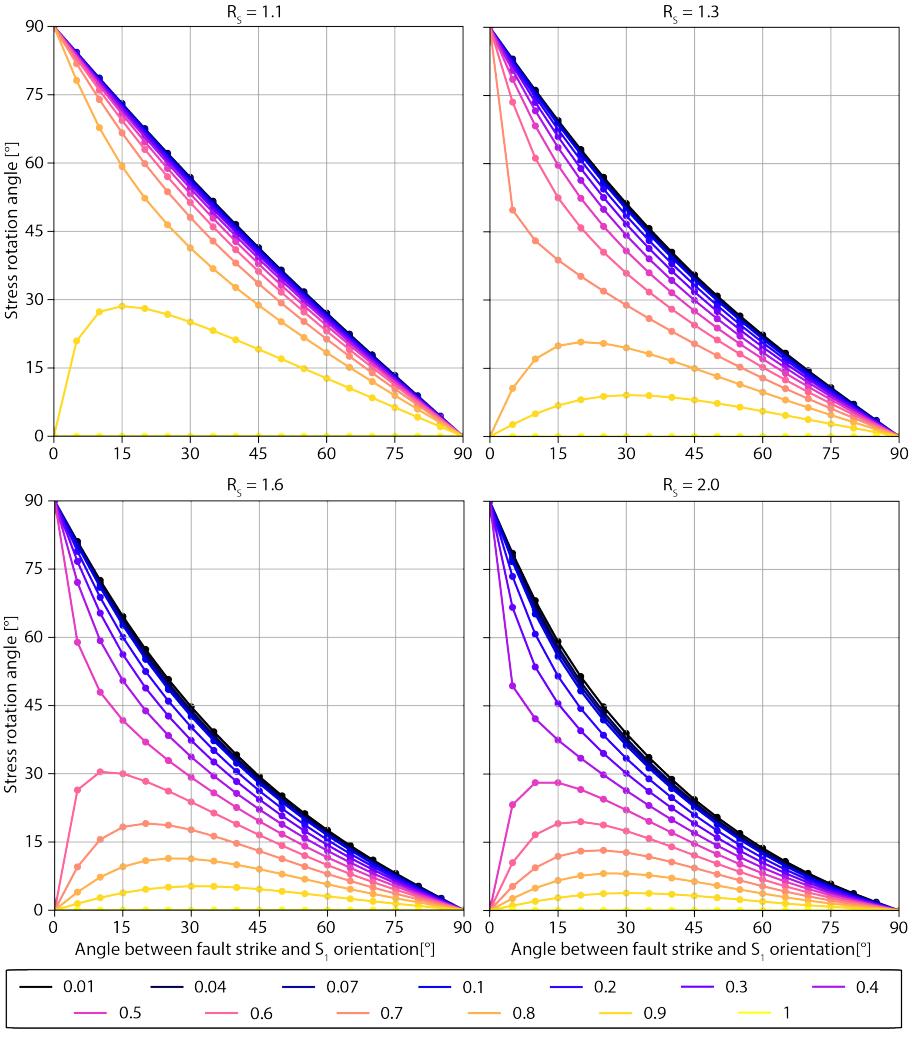

Figure 5. The dependence of stress rotation inside the fault core (y-axes) on the angle γ between the fault strike and the far-field orientation of S_1 (x-axes), the stiffness contrast R_E between fault core and host rock (colour coded lines), and the stress ratio R_S (panels). The underlying data is provided in the supplementary material.

modelling approach that chooses a representation of faults by a different rock material, this shows that the damage zone - if it is observed and its extent known - needs to be included in terms of rock properties.

4.4 Comparison of well data with the modelling results

Rotations of the S_{Hmax} orientation associated with changes in rock stiffness are mainly observed in boreholes, e.g. by rotating borehole breakouts or drilling induced tensile fractures (Brudy et al., 1997; Cui et al., 2014; Haimson et al., 2010; Hickman and Zoback, 2004; Lin et al., 2007; Massiot et al., 2019). Some notable examples are shown in Table 3. The observation is

https://doi.org/10.5194/egusphere-2024-1109
Preprint. Discussion started: 17 April 2024
© Author(s) 2024. CC BY 4.0 License.

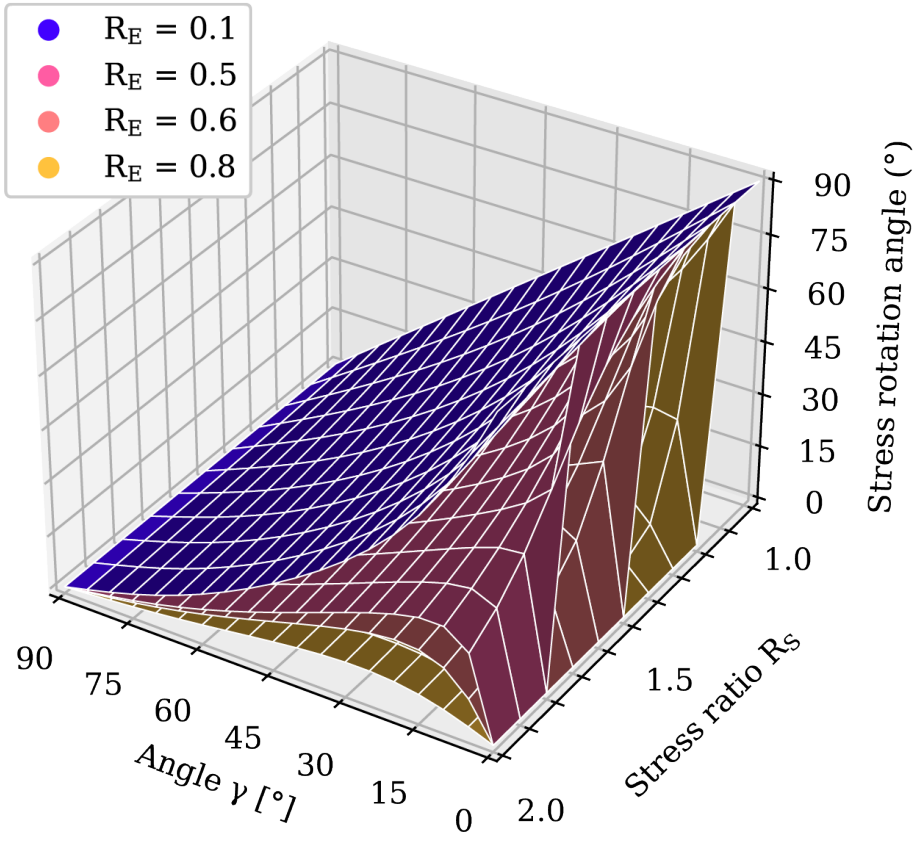

Figure 6. 3D representation of the stress rotation (z-axis) and its dependecy on the stiffness contrast R_E (color-coded planes), angle γ between fault and S_1 orientation (x-axis), and the stress ratio R_S (y-axis).

inherently subject to uncertainties due to the need for breakouts or drilling induced tensile fractures to occur in order to be able to identify a rotation. Thus, the number of significant observations of rotations is rather small and for some projects no rotation at the fault can be observed (Brodsky et al., 2017).

Massiot et al. (2019) observe significant rotations of the S_{Hmax} orientation in the Taranaki Basin offshore New Zealand. Most prominently a 30° rotation is observed at the intersection of the borehole Whio-1 with the almost vertically dipping Whio-1-fault. In this setting the orientation of S_{Hmax} is approximately parallel to the strike of aforementioned fault (Massiot et al., 2019; Rajabi et al., 2016c). The prevailing stress state is classified as close to transtensional ($S_{Hmax} \geq S_v > S_{hmin}$) with all three stress components inferred. This allows to estimate a preferential differential stress of 9 MPa which corresponds to a stress ratio of R_S=1.2 albeit uncertainties of up to 18MPa have to be considered in the stress components (Massiot et al., 2019). This information allows to use the herein estimated relations to derive a value for the stiffness contrast of R_E=0.8.

Further observations can be made for steeply dipping faults for example at the San Andreas Fault Observatory Drilling (SAFOD) (Hickman and Zoback, 2004) or the Wenchuan fault drilling (Cui et al., 2014) (Table 3). At the SAFOD drilling site,

https://doi.org/10.5194/egusphere-2024-1109
Preprint. Discussion started: 17 April 2024
© Author(s) 2024. CC BY 4.0 License.

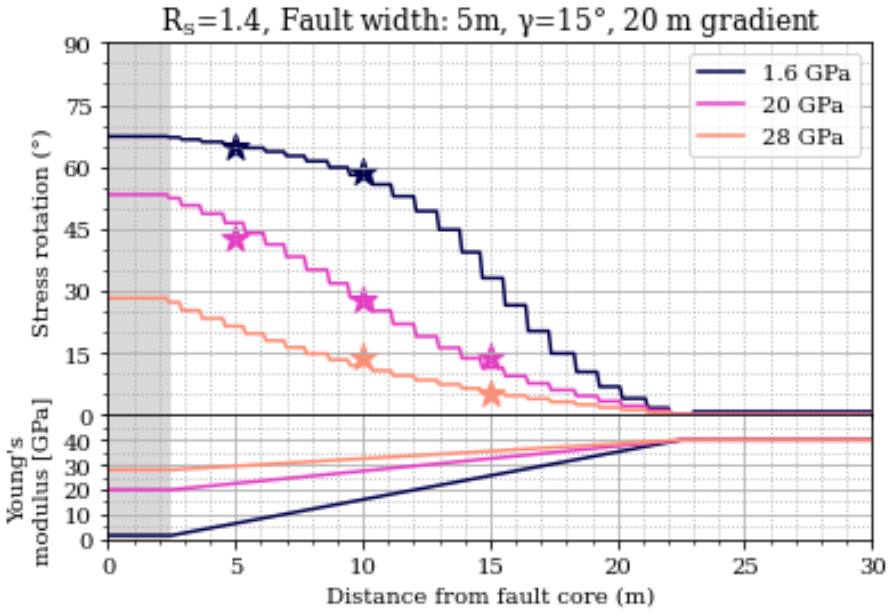

Figure 7. Stress rotation in the vicinity of a fault (top) with different fault stiffness (colour coded lines) in contrast to the same host rock stiffness of 40 GPa with a stress ratio R_S=1.4 and an angle γ=15°. The damage zone of the fault is realised by an increase of stiffness over 20 m (bottom). The stress rotation angles expected according to the presented study (Figure 5) without a gradient of rock stiffness are indicated (stars).

a differential stress of 64 MPa (R_S=2.2) is expected with an angle between fault strike and S_{Hmax} orientation of 50° (Hickman and Zoback, 2004). According to the herein presents approach, this limits the stress rotation to approx. 30° and requires a high stiffness contrast of R_E<0.1 (Table 3). This is in agreement with observations (Zoback et al., 2010).

At the Wenchuan fault drilling project stress rotations of up to 20° are observed. A large angle between fault strike and S_{Hmax} orientation and a small stress ratio (Cui et al., 2014) call for a rather moderate rock stiffness contrast of R_E<0.7 in order to explain the observed stress rotation angles (Table 3).

Eventually, at the German Continental Deep Drilling site (KTB) stress rotations are observed in unprecedented depths >7000m (Brudy et al., 1997). There, a rotation of 60° is observed in with accordingly high estimated stress magnitudes and also a high differential stress of 175 MPa and a stress ratio of R_S=2.4 (Brudy et al., 1997). The small angle between fault strike and S_{Hmax} orientation allows such a rotation to occur, even though $R_E \leq 0.3$ is required according to our generic approach.

The Taiwan Chelungpu Drilling Project (TCDP) drilled into the 30° dipping Chelungpu Fault which hosted the 1999 Chi-Chi earthquake (Hung et al., 2007; Lin et al., 2007). Stress rotations of up to 90° have been observed in the vicinity of the fault (Lin et al., 2007). Inferred differential stress and stress ratio, rock stiffness contrast and the observed stress rotation of 90° are well in agreement (Table 3). However, the angle γ = 90° between S_{Hmax} and fault strike should prohibit any stress rotation at

https://doi.org/10.5194/egusphere-2024-1109
Preprint. Discussion started: 17 April 2024
© Author(s) 2024. CC BY 4.0 License.

Table 3. Observed stress rotations and associated parameters. Parameters in italics are derived according to the herein presented approach.

Location	S_1-S_3 [MPa]	R_S	R_E	S_{Hmax} vs. Fault Strike	Stress rotation	Fault Dip angle	Reference
Agreement							
1. Taranaki Basin	6	1.2	0.8	0°	30°	90°	1
2. SAFOD	64	2.2	<0.1	50°	30°	70° - 90°	2
3. Wenchuan Fault	4-14	1.3-1.8	<0.7	69°	<20°	70°- 90°	3
4. KTB	175	2.4	<0.3	0°	60°	70° - 80°	4
Disagreement							
5. Chelungpu fault	24 - 36	1.75 – 2.8	0.6 -0.7	90°	90°	30°	5,6

1 Massiot et al. (2019), 2 Hickman and Zoback (2004), 3 Cui et al. (2014), 4 Brudy et al. (1997), 5 Lin et al. (2007), 6 Haimson et al. (2010)

all. Interestingly, this is the only regarded fault in Table 3 which is not steeply dipping which may indicate the relevance of the intermediate principal stress component and the need to investigate the stress rotation in a full 3D modelling approach.

4.5 Limitations

This failure of the generically derived relations to predict the expected stress rotation of 90° at the Chelungpu Fault (Table 3) indicates a limitation of the approach. The behaviour of any faults that have a significant deviation from a vertical to subvertical dip apparently do not follow the proposed scheme. This is expected to be a result of its limitation to two dimensions even though the generically modelled fault strike could also represent the dip. That shows the influence of the intermediate principal stress which cannot be investigated in a 2D model. Furthermore, the observed rotation of the S_{Hmax} orientation is only a part of the actual rotation which likely concerns all principal stress component's magnitude and orientation, as observed by the analysis of focal mechanism solutions in a temporal domain e.g. by Martínez-Garzón et al. (2013, 2014). This indicates the necessity to extend the presented approach to the full 3D stress tensor. This should be the aim of future studies as it is well beyond the scope of this work.

We aim to investigate of the influence of a rock stiffness contrast on a spatially homogeneous far field stress state. Our investigation addresses the rock stiffness contrast as the main driver for stress rotation. This contrasts with other studies which model an explicit fault that is able to slide (Hergert et al., 2015; Reiter et al., 2024). Therefore, the herein obtained results are not only valid for an interseismically locked fault that is weakened compared to the host rock but also for other rock stiffness contrasts.

Generally, most of our knowledge on the stress rotations at smaller scales are from the interpretation of borehole image logs. However, such rotations could not be seen in all cases, mainly due to the uncertainties in borehole image log interpretation, in particular when it comes to the analysis of borehole breakouts (Azzola et al., 2019; Kingdon et al., 2016). Borehole breakouts are defined as a significant section of the borehole wall that spalls off (Aadnoy and Bell, 1998). In some cases, where breakouts are wide (i.e., opening angles of 15° - 30°) it could be difficult to observe rotation <30° (Aadnoy and Bell, 1998). While

https://doi.org/10.5194/egusphere-2024-1109
Preprint. Discussion started: 17 April 2024
© Author(s) 2024. CC BY 4.0 License.

rotation angles >30° can be observed easier using breakouts a higher certainty in observations is expected for drilling induced tensile fractures, which are usually described as thin (sub)vertical fractures, in vertical boreholes (Aadnoy and Bell, 1998). However, they are less frequently observed and harder to interpret and may be misinterpreted as incipient breakouts in some cases (Rajabi et al., 2017b). In addition, borehole breakouts and/or drilling induced tensile fractures need to form in the first place both in the host rock and in the contrasting material in order to be able to detect a rotation at all. Thus, the detection of a stress rotation and even more so the estimation of the material contrast always is subject to uncertainties.

4.6 Other reasons for stress rotations

The presented approach in this study investigates elastic rock stiffness contrast as the primary reason for stress rotations. Alternatively, lithological units can be mechanically decoupled at a certain horizon due to a contrasting lithology. This also results in a perceived stress rotation in terms of different stress orientations above and below the respective horizon (Cornet and Röckel, 2012; Roth and Fleckenstein, 2001). These changes in rock properties e.g., in intrusions but also due to faults can cause massive changes in the S_{Hmax} orientation of up to 90° (Ahlers et al., 2018; Cornet and Röckel, 2012; Rajabi et al., 2024; Reiter, 2021; Tingay et al., 2011). However, the different angles of S_{Hmax} could be rather inherited remnant stresses instead of local deviations due to material contrasts. In other cases, stress rotations cannot be attributed to a specific cause (Wang et al., 2023) or anisotropies are assumed (Sahara et al., 2014; Wang et al., 2022). As such, they are not covered by the presented work.

Furthermore, this study does not concern temporal variations of the stress tensor. Such rotations can naturally occur co-seismically or post-seismically due to large magnitude natural earthquakes (Hardebeck, 2017; Hardebeck and Okada, 2018; King et al., 1994). Furthermore, temporal back-and-forth rotation of the principal stress components have been observed (Martínez-Garzón et al., 2013, 2014) and related to reservoir operations such as injection of fluids (Ziegler et al., 2017) as well, excavation works such as mining or tunnelling (Eberhardt, 2001; Ziegler et al., 2015).

5 Conclusions

We investigate the relationship between stress rotation in a fault with 1) a variable rock stiffness contrast, 2) the stress ratio of the far field, and 3) the far field stress orientation using a 2D plane strain model. Stress rotation is promoted by a low stress ratio and a low angle between the far field stress orientation and the fault strike. A high stiffness contrast further increases the stress rotation angle. According to this study, no stress rotation is possible for faults that are striking perpendicular to the maximum principal stress orientation. Faults parallel to the maximum principal stress orientation, however, experience either no stress rotation or a 90° stress rotation dependent on the stress ratio and the rock stiffness contrast within the fault core/damage zone. The established relations agree with observations from various scientific boreholes worldwide. However, they are only valid for steeply dipping faults where the intermediate principal stress component only has a minor effect. A fully 3D investigation of the established relations should be addressed in future research.

https://doi.org/10.5194/egusphere-2024-1109
Preprint. Discussion started: 17 April 2024
© Author(s) 2024. CC BY 4.0 License.

Data availability. All modelling results are available in the supporting material.

Author contributions. Conception and study design: RS, TN, MZ, LR, BM. Software: TN, MZ, RS. Interpretation & Discussion: all authors contributed equally. Writing: MZ, OH, RS

Competing interests. The authors declare that they have no competing interests,

Acknowledgements. The work leading to these results has received funding from the German Research Foundation (DFG grant PHYSALIS 523456847), BGE SpannEnD 2.0 project, RI Fabrice Cotton and from the Federal Ministry for the Environment, Nature Conservation, Nuclear Safety and Consumer Protection through project SQuaRe (project number: 02E12062C). Contributions by MR were made under his ARC Discovery Early Career Researcher Award (award number DE200101361).

https://doi.org/10.5194/egusphere-2024-1109
Preprint. Discussion started: 17 April 2024
© Author(s) 2024. CC BY 4.0 License.

References

Aadnoy, B. S. and Bell, J. S.: Classification Of Drilling-induced Fractures And Their Relationship To In-situ Stress Directions, The Log Analyst, 39, 1998.

Ahlers, S., Hergert, T., and Henk, A.: Numerical Modelling of Salt-Related Stress Decoupling in Sedimentary Basins–Motivated by Observational Data from the North German Basin, Geosciences 2019, Vol. 9, Page 19, 9, 19, https://doi.org/10.3390/GEOSCIENCES9010019, 2018.

Ahlers, S., Röckel, L., Hergert, T., Reiter, K., Heidbach, O., Henk, A., Müller, B., Morawietz, S., Scheck-Wenderoth, M., and Anikiev, D.: The crustal stress field of Germany: a refined prediction, Geothermal Energy, 10, 10, https://doi.org/10.1186/s40517-022-00222-6, 2022.

Azzola, J., Valley, B., Schmittbuhl, J., and Genter, A.: Stress characterization and temporal evolution of borehole failure at the Rittershoffen geothermal project, Solid Earth, 10, 1155–1180, https://doi.org/10.5194/se-10-1155-2019, 2019.

Barton, C. A. and Zoback, M. D.: Stress perturbations associated with active faults penetrated by boreholes: Possible evidence for near-complete stress drop and a new technique for stress magnitude measurement, Journal of Geophysical Research: Solid Earth, 99, 9373–9390, https://doi.org/10.1029/93JB03359, 1994.

Barton, C. A., Zoback, M. D., and Moos, D.: Fluid flow along potentially active faults in crystalline rock, Geology, 23, 683, https://doi.org/10.1130/0091-7613(1995)023<0683:FFAPAF>2.3.CO;2, 1995.

Bell, J. and Gough, D.: Northeast-southwest compressive stress in Alberta evidence from oil wells, Earth and Planetary Science Letters, 45, 475–482, https://doi.org/10.1016/0012-821X(79)90146-8, 1979.

Brodsky, E. E., Saffer, D., Fulton, P., Chester, F., Conin, M., Huffman, K., Moore, J. C., and Wu, H.: The postearthquake stress state on the Tohoku megathrust as constrained by reanalysis of the JFAST breakout data, Geophysical Research Letters, 44, 8294–8302, https://doi.org/10.1002/2017GL074027, 2017.

Brudy, M., Zoback, M. D., Fuchs, K., Rummel, F., and Baumgaertner, J.: Estimation of the complete stress tensor to 8 km depth in the KTB scientific drill holes' Implications for crustal strength, JOURNAL OF GEOPHYSICAL RESEARCH, 102, 453–471, https://doi.org/10.1029/96JB02942, 1997.

Cai, W., Zhu, H., and Liang, W.: Three-dimensional stress rotation and control mechanism of deep tunneling incorporating generalized Zhang–Zhu strength-based forward analysis, Engineering Geology, 308, 106 806, https://doi.org/10.1016/j.enggeo.2022.106806, 2022.

Casey, M.: Mechanics of shear zones in isotropic dilatant materials, Journal of Structural Geology, 2, 143–147, https://doi.org/10.1016/0191-8141(80)90044-9, 1980.

Catalli, F., Meier, M. A., and Wiemer, S.: The role of Coulomb stress changes for injection-induced seismicity: The Basel enhanced geothermal system, Geophysical Research Letters, 40, 72–77, https://doi.org/10.1029/2012GL054147, 2013.

Clavijo, S. P., Dash, A., Baby, G., Alafifi, A. M., and Finkbeiner, T.: Modeling principal stress orientations in the Arabian Plate using plate velocities, Geological Society, London, Special Publications, 546, https://doi.org/10.1144/SP546-2022-327, 2024.

Cornet, F. H. and Röckel, T.: Vertical stress profiles and the significance of "stress decoupling", Tectonophysics, 581, 193–205, https://doi.org/10.1016/J.TECTO.2012.01.020, 2012.

Cui, J., Lin, W., Wang, L., Gao, L., Huang, Y., Wang, W., Sun, D., Li, Z., Zhou, C., Qian, H., Peng, H., Xia, K., and Li, K.: Determination of three-dimensional in situ stresses by anelastic strain recovery in Wenchuan Earthquake Fault Scientific Drilling Project Hole-1 (WFSD-1), Tectonophysics, 619-620, 123–132, https://doi.org/10.1016/j.tecto.2013.09.013, 2014.

https://doi.org/10.5194/egusphere-2024-1109
Preprint. Discussion started: 17 April 2024
© Author(s) 2024. CC BY 4.0 License.

Dart, R. and Swolfs, H.: Subparallel faults and horizontal-stress orientations: an evaluation of in-situ stresses inferred from elliptical wellbore enlargements, pp. 519–529, Elsevier, https://doi.org/10.1016/B978-0-444-88607-1.50041-3, 1992.

Eberhardt, E.: Numerical modelling of three-dimension stress rotation ahead of an advancing tunnel face, International Journal of Rock Mechanics and Mining Sciences, 38, 499–518, https://doi.org/10.1016/S1365-1609(01)00017-X, 2001.

Engelder, T.: Deviatoric stressitis: A virus infecting the Earth science community, Eos, Transactions American Geophysical Union, 75, 209–212, https://doi.org/10.1029/94EO00885, 1994.

Faulkner, D. R., Mitchell, T. M., Healy, D., and Heap, M. J.: Slip on 'weak' faults by the rotation of regional stress in the fracture damage zone, Nature, 444, 922–925, https://doi.org/10.1038/nature05353, 2006.

Faulkner, D. R., Jackson, C. A., Lunn, R. J., Schlische, R. W., Shipton, Z. K., Wibberley, C. A., and Withjack, M. O.: A review of recent developments concerning the structure, mechanics and fluid flow properties of fault zones, Journal of Structural Geology, 32, 1557–1575, https://doi.org/10.1016/J.JSG.2010.06.009, 2010.

Freymark, J., Bott, J., Cacace, M., Ziegler, M. O., and Scheck-Wenderoth, M.: Influence of the Main Border Faults on the 3D Hydraulic Field of the Central Upper Rhine Graben, Geofluids, 2019, https://doi.org/10.1155/2019/7520714, 2019.

Gaucher, E., Schoenball, M., Heidbach, O., Zang, A., Fokker, P. A., Wees, J. D. V., and Kohl, T.: Induced seismicity in geothermal reservoirs: A review of forecasting approaches, https://doi.org/10.1016/j.rser.2015.08.026, 2015.

Gilmore, K. A., Sahu, C. K., Benham, G. P., Neufeld, J. A., and Bickle, M. J.: Leakage dynamics of fault zones: experimental and analytical study with application to CO2 storage, Journal of Fluid Mechanics, 931, A31, https://doi.org/10.1017/JFM.2021.970, 2022.

Gradmann, S., Olesen, O., Keiding, M., and Maystrenko, Y.: The 3D stress field of Nordland, northern Norway - insights from numerical modelling, Geological Society, London, Special Publications, 546, https://doi.org/10.1144/SP546-2023-163, 2024.

Haimson, B., Lin, W., Oku, H., Hung, J. H., and Song, S. R.: Integrating borehole-breakout dimensions, strength criteria, and leak-off test results, to constrain the state of stress across the Chelungpu Fault, Taiwan, Tectonophysics, 482, 65–72, https://doi.org/10.1016/J.TECTO.2009.05.016, 2010.

Han, C., Huang, Z., Xu, M., Wang, L., Mi, N., Yu, D., and Li, H.: Focal mechanism and stress field in the northeastern Tibetan Plateau: insight into layered crustal deformations, Geophysical Journal International, 218, 2066–2078, https://doi.org/10.1093/gji/ggz267, 2019.

Hardebeck, J. L.: The spatial distribution of earthquake stress rotations following large subduction zone earthquakes, Earth, Planets and Space, 69, https://doi.org/10.1186/s40623-017-0654-y, 2017.

Hardebeck, J. L. and Okada, T.: Temporal Stress Changes Caused by Earthquakes: A Review, https://doi.org/10.1002/2017JB014617, 2018.

Healy, D. and Hicks, S. P.: De-risking the energy transition by quantifying the uncertainties in fault stability, Solid Earth, 13, 15–39, https://doi.org/10.5194/se-13-15-2022, 2022.

Heidbach, O., Rajabi, M., Cui, X., Fuchs, K., Müller, B., Reinecker, J., Reiter, K., Tingay, M., Wenzel, F., Xie, F., Ziegler, M. O., Zoback, M.-L., and Zoback, M.: The World Stress Map database release 2016: Crustal stress pattern across scales, Tectonophysics, 744, 484–498, https://doi.org/10.1016/j.tecto.2018.07.007, 2018.

Henk, A.: Chapter 4 - Numerical modelling of faults, pp. 147–165, Elsevier, ISBN 978-0-12-815985-9, https://doi.org/https://doi.org/10.1016/B978-0-12-815985-9.00004-7, 2020.

Hergert, T., Heidbach, O., Reiter, K., Giger, S. B., and Marschall, P.: Stress field sensitivity analysis in a sedimentary sequence of the Alpine foreland, northern Switzerland, Solid Earth, 6, 533–552, https://doi.org/10.5194/se-6-533-2015, 2015.

Hickman, S. and Zoback, M.: Stress orientations and magnitudes in the SAFOD pilot hole, Geophysical Research Letters, 31, https://doi.org/10.1029/2004GL020043, 2004.

https://doi.org/10.5194/egusphere-2024-1109
Preprint. Discussion started: 17 April 2024
© Author(s) 2024. CC BY 4.0 License.

Holdsworth, R. E., Diggelen, E. W. E. V., Spiers, C. J., Bresser, J. H. P. D., Walker, R. J., and Bowen, L.: Fault rocks from the SAFOD core samples: Implications for weakening at shallow depths along the San Andreas Fault, California, Journal of Structural Geology, https://doi.org/10.1016/j.jsg.2010.11.010, 2010.

Homberg, C., Hu, J. C., Angelier, J., Bergerat, F., and Lacombe, O.: Characterization of stress perturbations near major fault zones: insights from 2-D distinct-element numerical modelling and field studies (Jura mountains), Journal of Structural Geology, 19, 703–718, https://doi.org/10.1016/S0191-8141(96)00104-6, 1997.

Hung, J.-H., Ma, K.-F., Wang, C.-Y., Ito, H., Lin, W., and Yeh, E.-C.: Subsurface structure, physical properties, fault-zone characteristics and stress state in scientific drill holes of Taiwan Chelungpu Fault Drilling Project, Tectonophysics, 466, 307–321, https://doi.org/10.1016/j.tecto.2007.11.014, 2007.

Isaacs, A. J., Evans, J. P., Kolesar, P. T., and Nohara, T.: Composition, microstructures, and petrophysics of the Mozumi fault, Japan: In situ analyses of fault zone properties and structure in sedimentary rocks from shallow crustal levels, Journal of Geophysical Research: Solid Earth, 113, https://doi.org/10.1029/2007JB005314, 2008.

King, C. P., Stein, R. O. S. S. S., and Lin, J.: Static Stress Changes and the Triggering of Earthquakes, Bulletin of the Seismological Society of America, 84, 935–953, https://doi.org/10.1785/BSSA0840030935, 1994.

Kingdon, A., Fellgett, M. W., and Williams, J. D.: Use of borehole imaging to improve understanding of the in-situ stress orientation of Central and Northern England and its implications for unconventional hydrocarbon resources, Marine and Petroleum Geology, 73, 1–20, https://doi.org/10.1016/j.marpetgeo.2016.02.012, 2016.

Kirsch, E.: Die Theorie der Elastizität und die Bedürfnisse der Festigkeitslehre, Zeitschrift des Vereines deutscher Ingenieure, 42, 1898.

Konrad, F., Savvatis, A., Degen, D., Wellmann, F., Einsiedl, F., and Zosseder, K.: Productivity enhancement of geothermal wells through fault zones: Efficient numerical evaluation of a parameter space for the Upper Jurassic aquifer of the North Alpine Foreland Basin, Geothermics, 95, 102 119, https://doi.org/10.1016/J.GEOTHERMICS.2021.102119, 2021.

Konstantinou, K. I., Mouslopoulou, V., Liang, W. T., Heidbach, O., Oncken, O., and Suppe, J.: Present-day crustal stress field in Greece inferred from regional-scale damped inversion of earthquake focal mechanisms, Journal of Geophysical Research: Solid Earth, 122, 506–523, https://doi.org/10.1002/2016JB013272, 2017.

Konstantinovskaya, E., Malo, M., and Castillo, D.: Present-day stress analysis of the St. Lawrence Lowlands sedimentary basin (Canada) and implications for caprock integrity during CO2 injection operations, Tectonophysics, 518-521, 119–137, https://doi.org/10.1016/j.tecto.2011.11.022, 2012.

Levi, N., Habermueller, M., Exner, U., Piani, E., Wiesmayr, G., and Decker, K.: The stress field in the frontal part of the Eastern Alps (Austria) from borehole image log data, Tectonophysics, 769, 228 175, https://doi.org/10.1016/J.TECTO.2019.228175, 2019.

Li, H., Wang, H., Xu, Z., Si, J., Pei, J., Li, T., Huang, Y., Song, S.-R., Kuo, L.-W., Sun, Z., Chevalier, M.-L., and Liu, D.: Characteristics of the fault-related rocks, fault zones and the principal slip zone in the Wenchuan Earthquake Fault Scientific Drilling Project Hole-1 (WFSD-1), Tectonophysics, https://doi.org/10.1016/j.tecto.2012.08.021, 2012.

Li, P., Cai, M., Gorjian, M., Ren, F., Xi, X., and Wang, P.: Interaction between in situ stress states and tectonic faults: A comment, International Journal of Minerals, Metallurgy and Materials, 30, 1227–1243, https://doi.org/10.1007/S12613-023-2607-8/METRICS, 2023.

Lin, W., Yeh, E.-C., Ito, H., Hirono, T., Soh, W., Wang, C.-Y., Ma, K.-F., Hung, J.-H., and Song, S.-R.: Preliminary Results of Stress Measurement Using Drill Cores of TCDP Hole-A: an Application of Anelastic Strain Recovery Method to Three-Dimensional In-Situ Stress Determination, Terr. Atmos. Ocean. Sci, 18, 380, https://doi.org/10.3319/TAO.2007.18.2.379(TCDP), 2007.

https://doi.org/10.5194/egusphere-2024-1109
Preprint. Discussion started: 17 April 2024
© Author(s) 2024. CC BY 4.0 License.

Lin, W., Yeh, E.-C., Hung, J.-H., Haimson, B., and Hirono, T.: Localized rotation of principal stress around faults and fractures determined from borehole breakouts in hole B of the Taiwan Chelungpu-fault Drilling Project (TCDP), Tectonophysics, 482, 82–91, https://doi.org/10.1016/j.tecto.2009.06.020, 2010.

Lockner, D. A., Tanaka, H., Ito, H., Ikeda, R., Omura, K., and Naka, H.: Geometry of the Nojima fault at Nojima-Hirabayashi, Japan - I. A simple damage structure inferred from borehole core permeability, Pure and Applied Geophysics, 166, 1649–1667, https://doi.org/10.1007/S00024-009-0515-0/METRICS, 2009.

Long, J. C. and Ewing, R. C.: YUCCA MOUNTAIN: Earth-Science Issues at a Geologic Repository for High-Level Nuclear Waste, Annual Review of Earth and Planetary Sciences, 32, 363–401, https://doi.org/10.1146/annurev.earth.32.092203.122444, 2004.

Martínez-Garzón, P., Bohnhoff, M., Kwiatek, G., and Dresen, G.: Stress tensor changes related to fluid injection at the Geysers geothermal field, California, Geophysical Research Letters, 40, 2596–2601, https://doi.org/10.1002/grl.50438, 2013.

Martínez-Garzón, P., Kwiatek, G., Sone, H., Bohnhoff, M., Dresen, G., and Hartline, C.: Spatiotemporal changes, faulting regimes, and source parameters of induced seismicity: A case study from the Geysers geothermal field, Journal of Geophysical Research: Solid Earth, 119, 8378–8396, https://doi.org/10.1002/2014JB011385, 2014.

Massiot, C., Seebeck, H., Nicol, A., McNamara, D. D., Lawrence, M. J., Griffin, A. G., Thrasher, G. P., O'Brien, G., and Viskovic, G. P. D.: Effects of regional and local stresses on fault slip tendency in the southern Taranaki Basin, New Zealand, Marine and Petroleum Geology, 107, 467–483, https://doi.org/10.1016/J.MARPETGEO.2019.05.030, 2019.

Morris, A., Ferrill, D. A., and Henderson, D. B.: Slip-tendency analysis and fault reactivation, Geology, 24, 275, https://doi.org/10.1130/0091-7613(1996)024<0275:STAAFR>2.3.CO;2, 1996.

Mukherjee, S., Rajabi, M., Esterle, J., and Copley, J.: Subsurface fractures, in-situ stress and permeability variations in the Walloon Coal Measures, eastern Surat Basin, Queensland, Australia, International Journal of Coal Geology, 222, 103 449, https://doi.org/10.1016/J.COAL.2020.103449, 2020.

Müller, B., Schilling, F., Röckel, T., and Heidbach, O.: Induced Seismicity in Reservoirs: Stress Makes the Difference Induzierte, Erdöl Erdgas Kohle, https://doi.org/10.19225/180106, 2018.

Niederhuber, T., Kruszewski, M., Röckel, T., Rische, M., Alber, M., and Müller, B.: Stress orientations from hydraulic fracturing tests in the Ruhr area in comparison to stress orientations from borehole observations and earthquake focal mechanisms, Zeitschrift der Deutschen Gesellschaft für Geowissenschaften, 173, 625–635, https://doi.org/10.1127/zdgg/2022/0352, 2023.

Ptáček, J., Konicek, P., Staš, L., Waclawik, P., and Kukutsch, R.: Rotation of principal axes and changes of stress due to mine-induced stresses, Canadian Geotechnical Journal, 52, 1440–1447, https://doi.org/10.1139/cgj-2014-0364, 2015.

Rajabi, M., Tingay, M., and Heidbach, O.: The present-day state of tectonic stress in the Darling Basin, Australia: Implications for exploration and production, Marine and Petroleum Geology, 77, 776–790, https://doi.org/10.1016/j.marpetgeo.2016.07.021, 2016a.

Rajabi, M., Tingay, M., and Heidbach, O.: The present-day stress field of New South Wales, Australia, Australian Journal of Earth Sciences, 63, 1–21, https://doi.org/10.1080/08120099.2016.1135821, 2016b.

Rajabi, M., Ziegler, M. O., Tingay, M., Heidbach, O., and Reynolds, S.: Contemporary tectonic stress pattern of the Taranaki Basin, New Zealand, Journal of Geophysical Research: Solid Earth, 121, 6053–6070, https://doi.org/10.1002/2016JB013178, 2016c.

Rajabi, M., Tingay, M., Heidbach, O., Hillis, R., and Reynolds, S.: The present-day stress field of Australia, https://doi.org/10.1016/j.earscirev.2017.04.003, 2017a.

Rajabi, M., Tingay, M., King, R., and Heidbach, O.: Present-day stress orientation in the Clarence-Moreton Basin of New South Wales, Australia: a new high density dataset reveals local stress rotations, Basin Research, 29, 622–640, https://doi.org/10.1111/bre.12175, 2017b.

https://doi.org/10.5194/egusphere-2024-1109
Preprint. Discussion started: 17 April 2024
© Author(s) 2024. CC BY 4.0 License.

Rajabi, M., Esterle, J., Heidbach, O., Travassos, D., and Fumo, S.: Characterising the contemporary stress orientations near an active continental rifting zone: A case study from the Moatize Basin, central Mozambique, Basin Research, 34, 1292–1313, https://doi.org/10.1111/bre.12660, 2022.

Rajabi, M., Ziegler, M., Heidbach, O., Mukherjee, S., and Esterle, J.: Contribution of mine borehole data toward high-resolution stress mapping: An example from northern Bowen Basin, Australia, International Journal of Rock Mechanics and Mining Sciences, 173, 105 630, https://doi.org/10.1016/j.ijrmms.2023.105630, 2024.

Reinecker, J., Tingay, M., Müller, B., and Heidbach, O.: Present-day stress orientation in the Molasse Basin, Tectonophysics, 482, 129–138, https://doi.org/10.1016/j.tecto.2009.07.021, 2010.

Reiter, K.: Stress rotation – impact and interaction of rock stiffness and faults, Solid Earth, 12, 1287–1307, https://doi.org/10.5194/se-12-1287-2021, 2021.

Reiter, K., Heidbach, O., Schmitt, D., Haug, K., Ziegler, M. O., and Moeck, I.: A revised crustal stress orientation database for Canada, Tectonophysics, 636, 111–124, https://doi.org/10.1016/j.tecto.2014.08.006, 2014.

Reiter, K., Heidbach, O., and Ziegler, M. O.: Impact of faults on the remote stress state, Solid Earth, 15, 305–327, https://doi.org/10.5194/se-15-305-2024, 2024.

Roth, F. and Fleckenstein, P.: Stress orientations found in north-east Germany differ from the West European trend, Terra Nova, 13, 289–296, https://doi.org/10.1046/J.1365-3121.2001.00357.X, 2001.

Röckel, L., Ahlers, S., Müller, B., Reiter, K., Heidbach, O., Henk, A., Hergert, T., and Schilling, F.: The analysis of slip tendency of major tectonic faults in Germany, Solid Earth, 13, 1087–1105, https://doi.org/10.5194/se-13-1087-2022, 2022.

Sahara, D. P., Schoenball, M., Kohl, T., and Müller, B. I.: Impact of fracture networks on borehole breakout heterogeneities in crystalline rock, International Journal of Rock Mechanics and Mining Sciences, 71, 301–309, https://doi.org/10.1016/j.ijrmms.2014.07.001, 2014.

Schoenball, M., Dorbath, L., Gaucher, E., Wellmann, J. F., and Kohl, T.: Change of stress regime during geothermal reservoir stimulation, Geophysical Research Letters, 41, 1163–1170, https://doi.org/10.1002/2013GL058514, 2014.

Schoenball, M., Walsh, F. R., Weingarten, M., and Ellsworth, W. L.: How faults wake up: The Guthrie-Langston, Oklahoma earthquakes, The Leading Edge, 37, 100–106, https://doi.org/10.1190/tle37020100.1, 2018.

Seithel, R., Steiner, U., Müller, B., Hecht, C., and Kohl, T.: Local stress anomaly in the Bavarian Molasse Basin, Geothermal Energy, 3, https://doi.org/10.1186/s40517-014-0023-z, 2015.

Seithel, R., Gaucher, E., Mueller, B., Steiner, U., and Kohl, T.: Probability of fault reactivation in the Bavarian Molasse Basin, Geothermics, 82, 81–90, https://doi.org/10.1016/j.geothermics.2019.06.004, 2019.

Shamir, G. and Zoback, M. D.: Stress orientation profile to 3.5 km depth near the San Andreas Fault at Cajon Pass, California, Journal of Geophysical Research: Solid Earth, 97, 5059–5080, https://doi.org/10.1029/91JB02959, 1992.

Siler, D. L.: Structural discontinuities and their control on hydrothermal systems in the Great Basin, USA, Geoenergy, 1, https://doi.org/10.1144/geoenergy2023-009, 2023.

Snee, J. E. L. and Zoback, M. D.: State of stress in the Permian Basin, Texas and New Mexico: Implications for induced seismicity, The Leading Edge, 37, 127–134, https://doi.org/10.1190/TLE37020127.1, 2018.

Sonder, L. J.: EFFECTS OF DENSITY CONTRASTS ON THE ORIENTATION OF STRESSES IN THE LITHOSPHERE: RELATION TO PRINCIPAL STRESS DIRECTIONS IN THE TRANSVERSE RANGES, CALIFORNIA, 1990.

Spann, H., Müller, B., and Fuchs, K.: Interpretation of anomalies in observed stress data at the central graben (north sea) — numerical and analytical approach, Soil Dynamics and Earthquake Engineering, 13, 1–11, https://doi.org/10.1016/0267-7261(94)90036-1, 1994.

https://doi.org/10.5194/egusphere-2024-1109
Preprint. Discussion started: 17 April 2024
© Author(s) 2024. CC BY 4.0 License.

Talukdar, M., Sone, H., and Kuo, L.: Lithology and Fault-Related Stress Variations Along the TCDP Boreholes: The Stress State Before and After the 1999 Chi-Chi Earthquake, Journal of Geophysical Research: Solid Earth, 127, https://doi.org/10.1029/2021JB023290, 2022.

Tingay, M., Bentham, P., de Feyter, A., and Kellner, A.: Present-day stress-field rotations associated with evaporites in the offshore Nile Delta, Bulletin of the Geological Society of America, 123, 1171–1180, https://doi.org/10.1130/B30185.1, 2011.

Treffeisen, T. and Henk, A.: Representation of faults in reservoir-scale geomechanical finite element models – A comparison of different modelling approaches, Journal of Structural Geology, 131, 103 931, https://doi.org/10.1016/j.jsg.2019.103931, 2020.

Vadacca, L., Rossi, D., Scotti, A., and Buttinelli, M.: Slip Tendency Analysis, Fault Reactivation Potential and Induced Seismicity in the Val d'Agri Oilfield (Italy), Journal of Geophysical Research: Solid Earth, 126, https://doi.org/10.1029/2019JB019185, 2021.

van Wees, J.-D., Osinga, S., Thienen-Visser, K. V., and Fokker, P. A.: Reservoir creep and induced seismicity: inferences from geomechanical modeling of gas depletion in the Groningen field, Geophysical Journal International, 212, 1487–1497, https://doi.org/10.1093/gji/ggx452, 2018.

Wang, W., Schmitt, D. R., and Li, W.: A program to forward model the failure pattern around the wellbore in elastic and strength anisotropic rock formations, International Journal of Rock Mechanics and Mining Sciences, 151, 105 035, https://doi.org/10.1016/j.ijrmms.2022.105035, 2022.

Wang, W., Schmitt, D. R., and Chan, J.: Heterogeneity Versus Anisotropy and the State of Stress in Stable Cratons: Observations From a Deep Borehole in Northeastern Alberta, Canada, Journal of Geophysical Research: Solid Earth, 128, https://doi.org/10.1029/2022JB025287, 2023.

Wees, J. D. V., Orlic, B., Eijs, R. V., Zijl, W., Jongerius, P., Schreppers, G. J., Hendriks, M., and Cornu, . T.: Integrated 3D geomechanical modelling for deep subsurface deformation: a case study of tectonic and human-induced deformation in the eastern Netherlands, http://sp.lyellcollection.org/, 2003.

Williams, J. N., Toy, V. G., Massiot, E., Mcnamara, D. D., and Wang, T.: Damaged beyond repair? Characterising the damage zone of a fault late in its interseismic cycle, the Alpine Fault, New Zealand, Journal of Structural Geology, https://doi.org/10.1016/j.jsg.2016.07.006, 2016.

Worum, G., van Wees, J.-D., Bada, G., van Balen, R. T., Cloetingh, S., and Pagnier, H.: Slip tendency analysis as a tool to constrain fault reactivation: A numerical approach applied to three-dimensional fault models in the Roer Valley rift system (southeast Netherlands), Journal of Geophysical Research: Solid Earth, 109, https://doi.org/10.1029/2003JB002586, 2004.

Xing, H., Makinouchi, A., and Mora, P.: Finite element modeling of interacting fault systems, Physics of the Earth and Planetary Interiors, 163, 106–121, https://doi.org/10.1016/j.pepi.2007.05.006, 2007.

Yale, D. P.: Fault and stress magnitude controls on variations in the orientation of in situ stress, Geological Society, London, Special Publications, 209, 55–64, https://doi.org/10.1144/GSL.SP.2003.209.01.06, 2003.

Yamada, Y. and Shibanuma, J.: Small-scale stress fluctuations in borehole breakouts and their implication in identifying potential active faults around the seismogenic megasplay fault, Nankai Trough, SW Japan, Earth, Planets and Space, 67, 17, https://doi.org/10.1186/s40623-014-0176-9, 2015.

Zhang, S., Ma, X., Bröker, K., van Limborgh, R., Wenning, Q., Hertrich, M., and Giardini, D.: Fault Zone Spatial Stress Variations in a Granitic Rock Mass: Revealed by Breakouts Within an Array of Boreholes, Journal of Geophysical Research: Solid Earth, 128, https://doi.org/10.1029/2023JB026477, 2023.

Ziegler, M. O.: Rock Properties and Modelled Stress State Uncertainties: A Study of Variability and Dependence, Rock Mechanics and Rock Engineering, https://doi.org/10.1007/s00603-022-02879-8, 2022.

https://doi.org/10.5194/egusphere-2024-1109
Preprint. Discussion started: 17 April 2024
© Author(s) 2024. CC BY 4.0 License.

Ziegler, M. O., Reiter, K., Heidbach, O., Zang, A., Kwiatek, G., Stromeyer, D., Dahm, T., Dresen, G., and Hofmann, G.: Mining-Induced Stress Transfer and Its Relation to a Mw 1.9 Seismic Event in an Ultra-deep South African Gold Mine, Pure and Applied Geophysics, 172, 2557–2570, https://doi.org/10.1007/s00024-015-1033-x, 2015.

Ziegler, M. O., Heidbach, O., Reinecker, J., Przybycin, A. M., and Scheck-Wenderoth, M.: A multi-stage 3-D stress field modelling approach exemplified in the Bavarian Molasse Basin, Solid Earth, 7, 1365–1382, https://doi.org/10.5194/se-7-1365-2016, 2016a.

Ziegler, M. O., Heidbach, O., Reinecker, J., Przybycin, A. M., and Scheck-Wenderoth, M.: Corrigendum to "A multi-stage 3-D stress field modelling approach exemplified in the Bavarian Molasse Basin" published in Solid Earth, 7, 1365–1382, 2016, Solid Earth, 7, 1365–1382, https://doi.org/10.5194/se-7-1365-2016-corrigendum, 2016b.

Ziegler, M. O., Rajabi, M., Heidbach, O., Hersir, G. P., Ágústsson, K., Árnadóttir, S., and Zang, A.: The stress pattern of Iceland, Tectonophysics, 674, 101–113, https://doi.org/10.1016/j.tecto.2016.02.008, 2016c.

Ziegler, M. O., Heidbach, O., Zang, A., Martínez-Garzón, P., and Bohnhoff, M.: Estimation of the differential stress from the stress rotation angle in low permeable rock, Geophysical Research Letters, 44, 6761–6770, https://doi.org/10.1002/2017GL073598, 2017.

Ziegler, M. O., Heidbach, O., Morawietz, S., and Wang, Y.: Manual of the Matlab Script FAST Calibration v2.4, https://doi.org/10.48440/wsm.2023.002, 2023.

Zoback, M. D., Hickman, S., and Ellsworth, W.: Scientific Drilling Into the San Andreas Fault Zone, Eos, Transactions American Geophysical Union, 91, 197–199, https://doi.org/10.1029/2010EO220001, 2010.

Zoback, M. L.: First- and second-order patterns of stress in the lithosphere: The World Stress Map Project, Journal of Geophysical Research: Solid Earth, 97, 11 703–11 728, https://doi.org/10.1029/92JB00132, 1992.